JOURNAL OF AIR TRANSPORTATION
Vol. 26, No. 1, January 2018

Simultaneous Optimization of Airway and Sector Design for Air Traffic Management

T. K. Venugopalan,* Cheryl Sze Yin Wong,† S. Suresh,‡ and N. Sundararajan§
Nanyang Technological University, Singapore 639798, Republic of Singapore

DOI: 10.2514/1.D0090

Dynamic airspace sectorization is an evolving concept of balancing the workload of air traffic controllers by changing the area of airspace under the controller based on the traffic demands. Proposed methodologies in literature typically consider fixed air traffic routes. However, routing can be an alternative effective handle for balancing the controller workloads, especially when making pretactical decisions where the redesigning of sectors has limited flexibility. In this paper, an optimization framework called simultaneous optimization of airway and airspace is proposed for handling changing the availability of airspace due to weather disturbances or airspace restrictions. A scenario such as this involves the rerouting of air traffic, which creates an unexpected imbalance in workloads. The framework overcomes this imbalance by finding a reroute and resectorization strategy that minimize workload imbalance across sectors and maximize the sector similarity with original sector shapes. An experimental study is performed to compare this methodology with a sequential design approach; the concurrent consideration of the effect of sector redesign and flow rerouting on the design objectives yields better and more optimal solutions. Furthermore, the application of the proposed framework on the Singapore flight information region with historical flight data reflects similar conclusions.

Nomenclature

A	=	set of airways
a	=	sequence of waypoints of each airway
C	=	matrix of clearance distances
c	=	clearance distance between an airway and an airspace disturbance
cor	=	sector similarity ratio between old and new sectors
cp	=	crossing point between airways
$cWkl$	=	coordination workload of a sector
D	=	set of airspace disturbances
d	=	location of the center of an airspace disturbance
f	=	flow rate of an airway
min D	=	minimum distance of a crossing point from the sector boundaries
$mWkl$	=	monitoring workload of a sector
N	=	set of discretized airspace grids
n	=	location of an airspace grid
R	=	set of airway routes
$\hat{R}$	=	set of previously designed airway routes
r	=	route of an individual airway
rad	=	bounding circle radius of an airspace disturbance
s	=	sector
sectSim	=	sector similarity metric
V	=	set of Voronoi sites
v	=	location of a Voronoi site
w	=	location of a waypoint
x	=	mapping between new and old sectors
α	=	number of airways
β	=	number of waypoints within an airway
γ	=	number of airspace grids
δ	=	number of airspace disturbances
ϵ	=	scaling factor
η	=	number of airspace sectors
θ	=	binary value representing outgoing traffic flow
λ	=	longitude
ϕ	=	latitude
ψ	=	number of crossing points

Received 9 August 2017; revision received 10 February 2018; accepted for publication 12 February 2018; published online 28 February 2018.

*Research Assistant, School of Computer Science and Engineering.
†Ph.D. Student, School of Computer Science and Engineering.
‡Associate Professor, School of Computer Science and Engineering. Senior Member AIAA.
§SRF, School of Computer Science and Engineering. Associate Fellow AIAA.

I. Introduction

A TYPICAL air traffic control center monitors and ensures the safety of airborne flights. It is achieved by multiple air traffic controllers (ATCs), each of whom is designated a segment of airspace (a sector) under their control. The ATC adapts to the growing air traffic with varying densities [1,2]. Thus, there is a need to ensure that the workload is distributed evenly among all the ATCs, as well as maintained within permissible limits for every ATC. Using flight plans, one can divide the area of control between ATCs (sectorization) to ensure a near-even distribution of the workload. In the future, dynamic resectorization is likely to become an active strategy in balancing the traffic controller's workloads.

With flight plans made available days in advance, there is adequate time to plan and design optimal sectors. Thus, air traffic flow management (traffic routing) and sectorization are not naturally coupled problems due to the flexibility available in sectorization. The process of air traffic routing and airspace sector design is usually sequentially performed [3,4]. However, there are frequent scenarios of weather-impacted or -restricted airspaces, the knowledge of which is available to an air traffic control center (ATCC) only a few hours in advance. Performing a heuristic rerouting of air traffic to avoid flights through these regions causes imbalances in the workloads of ATCs. In this scenario, the flexibility in changing the areas of control of ATCs, or increasing the available manpower, is limited. These limitations make the routing and sectorization problems coupled, where it is also highly preferable to perform any rerouting by considering its impact on sectorization. Hence, there is a real need to look at the problem of simultaneous optimization of both sectorization and routing to minimize and balance the controller's workloads while also satisfying other sector or flow constraints.

The Dynamic Airspace Routing Tool (DART) is a large-scale simulation model for the U.S. National Airspace System (NAS) flow management used in several areas of research [5]. It is capable of incorporating various rerouting strategies to generate optimal routes that avoid both hazardous weather conditions as well as overloaded sectors. The sector shapes are considered fixed, and overloading of sectors is prevented purely through rerouting. Using both sector

design and flow management as options to prevent overloading of sectors, Klein et al. [6] investigated a dynamic airspace configuration/traffic flow management (DAC-TFM) strategy. They used the NAS airspace dynamic analysis and partitioning tool for the dynamic airspace configuration (DAC) combined with DART for the total flight management. They proposed a sequential strategy: first rerouting to avoid weather restrictions, followed by resectorization for the newly generated routes with sector capacity constraints in mind, and a final round of rerouting with the additional objective to avoid any overloaded sector. Due to the coupled nature of the problem, they also investigated an iterative approach of the DAC-TFM loop but found that it did not improve the solution. One may argue that this is the inherent problem associated with independently designing the sector shapes and routes by keeping one of them constant while designing the other.

To overcome the aforementioned problem, we propose an approach to simultaneously optimize both the sector design and flow rerouting, and it is carried out for en route airspace with restricted airspaces. The major contribution of this paper is in the development of a framework called simultaneous optimization of both airway and airspace (SAWAS). This framework incorporates the design objectives, such as balancing the ATC traffic monitoring workload, minimizing the ATC coordination workloads, and maximizing the similarity of sector shapes with a given sectorization. Furthermore, it includes sector design constraints to provide convex sector shapes and sector boundaries that are far from traffic flow crossing points. SAWAS concurrently considers the effects of rerouting and resectorization on the desired design objectives. SAWAS uses an evolutionary algorithm inspired by previous works [7]. As a result, it finds both the airspace sectors and reroute strategies that are satisfying the desired objectives. Furthermore, a novel algorithm has been developed for traffic rerouting, which is referred to as the conflict avoidance and airway redesign (CAARD) algorithm. This algorithm is used to design airways that follow specified waypoints, avoiding unavailable regions in the airspace. Furthermore, routing of multiple airways with minimal conflicts is also handled.

The performance of SAWAS has been evaluated first using a simulation, and it was next evaluated using real flight data from the Singapore flight information region (FIR). The simulation was based on popular airways in the Singapore airspace with equal flow rates. It illustrates how simultaneous management of airways and airspace produces more and better solutions than using a sequential method of rerouting and resectorization. The second study considers the current airways available in the upper airspace of the Singapore FIR, with estimated flow rates obtained from real flight data. With more airways, the feasibility of solutions becomes an issue with restricted airspaces. Based on both studies, SAWAS is able to provide the user with optimal solutions.

This paper is organized as follows. Section II describes the basic model of airspace and air traffic flow. Section III discusses the simultaneous optimization framework and its subcomponents for resectorization and rerouting. Section IV describes the performance evaluation of SAWAS based on two experimental studies. The first compares the proposed simultaneous optimization approach with a sequential optimization approach for a typical air traffic management scenario. The second study implements SAWAS in the busy Singapore FIR and evaluates its performance under a more realistic scenario. Finally, Sec. V summarizes the main conclusions of the paper.

II. Modeling of Airspace and Traffic Flow

Decision-making processes performed in a typical ATCC are categorized based on the frequency at which they are performed, i.e., strategic, pretactical, and tactical. Figure 1 illustrates the vision for introducing the use of dynamic sector shapes and airway routes into this framework. At the strategic stage, flight plans and knowledge based on past experiences are used to find the best sector shapes that balance the ATC workloads across all the sectors. At this stage, the airway route design is independent of the sectorization. At the pretactical stage, the sectorization and airways (designed at the strategic level) are modified based on the airspace restrictions and weather forecast data obtained by the ATCC. This modification is applied for a subsequent 2 to 6 h time window. This is the stage where the combined optimization of airway design and sectorization is envisioned to be beneficial. At the tactical stage, the individual aircraft pilot and the ATC coordinate to take immediate decisions regarding the flight. At this stage, the sectorization is frozen. Experiences acquired from implementing dynamic sector shapes and routes feed to a knowledge base that helps in future design preferences and decision making.

As an example, a simulated traffic flow pattern in Singapore's southern airspace consisting of three airways is shown in Fig. 2. The designed sectors with balanced ATC workloads for this traffic flow are also indicated. Consider a scenario in which a weather forecast indicates that airway 1 traffic flow will be affected by a weather disturbance (the red dotted circle). This calls for a reroute of the flow. To avoid the weather disturbance, the flow may be diverted either to the north or south of the disturbance. Each of these alternatives will cause a change in the workloads of neighboring sectors, and thus an imbalance in the overall workload distribution. One option is to design the reroute strategy first; after which, one can handle the imbalance in workloads through sector redesign. However, in this work, the aim is to develop a concurrent strategy involving both airspace and air route changes for results that minimize the sector workload imbalances.

A. Airspace Modeling

Constructed sector shapes are typically presented in two dimensions (latitude and longitude) or three dimensions (including the altitude). In the case of two-dimensional (2-D) representations, the shape is usually considered uniform for all altitude layers. Three-dimensional (3-D) construction, however, allows for more complex sector shapes, especially as required in the case of terminal airspace for which the sector shapes resemble an inverted wedding cake. The sectorization component in this paper considers designing the 2-D sectors for en route airspace. The sector shapes are generated through

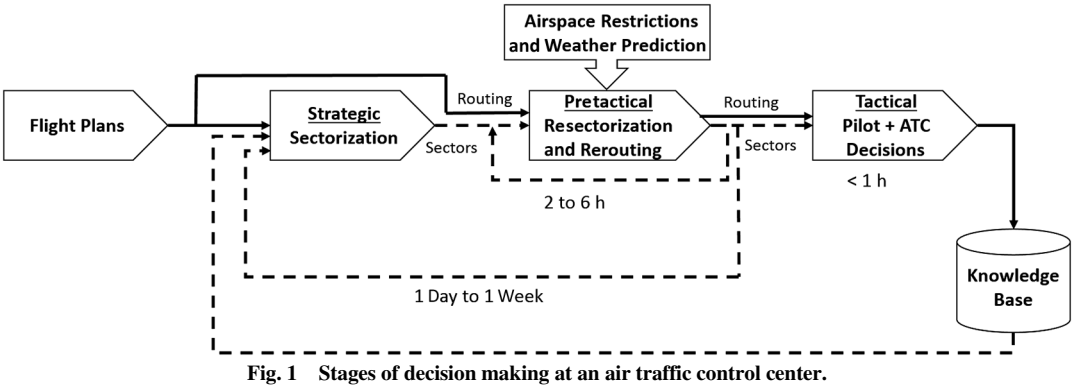

Fig. 1 Stages of decision making at an air traffic control center.

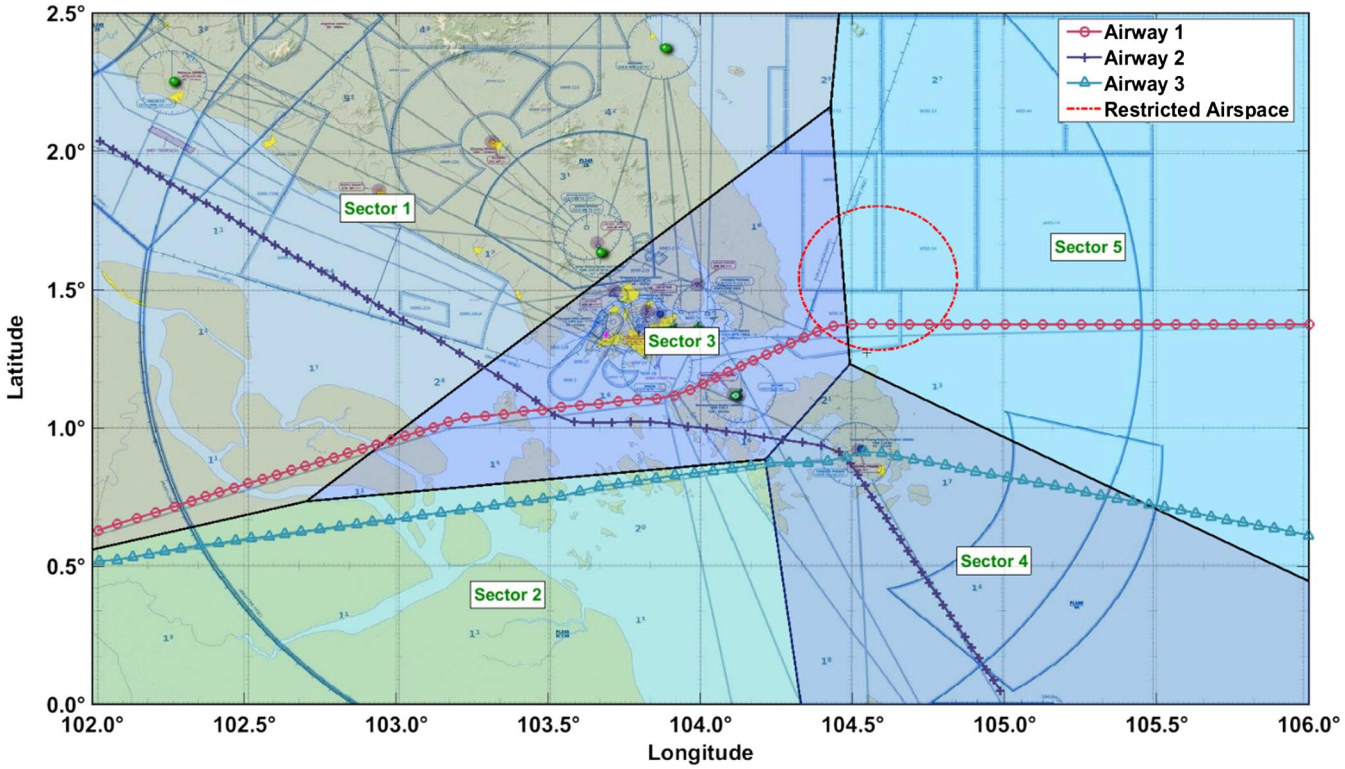

Fig. 2 Air traffic management scenario in Singapore airspace with airways and sectors indicated (source: SkyVector, 2015 (https://skyvector.com/)).

Voronoi diagrams [8,9]. Other techniques such as defining geometric equations to express the sector shapes, graph-based sector design, and expressing them as a cluster of fundamental airspace units also exist [10,11].

A Voronoi diagram is a partitioning technique subdividing a given region into subregions. A set of points known as sites is used to generate these partitions, satisfying the condition that any point within each partition is closest to its corresponding site. Such diagrams have an interesting property that the resulting shape of the partitions is strictly convex (internal angles are less than 180 deg). This has persuaded researchers to use this construction technique to generate sector shapes for which the convexities are always guaranteed. Furthermore, it allows for an elegant definition of the airspace sector as a set of coordinate points of its generating sites. However, a shortcoming of the use of Voronoi diagrams is that one cannot exhaustively generate all possible polygonal partitions of an airspace. This limitation can somewhat be alleviated by an iterative deepening technique [12], in which hierarchical partitioning gives rise to a larger variety of airspace partitions.

The set of sites used to generate the sector shapes is denoted as $V = \{\boldsymbol{v}_1, \boldsymbol{v}_2, \ldots, \boldsymbol{v}_\eta\}$, and $\boldsymbol{v}_i$ is

$$\boldsymbol{v}_i = \begin{pmatrix} v_i^\lambda \\ v_i^\phi \end{pmatrix} \qquad i = 1, \ldots, \eta \tag{1}$$

where η is the number of sectors being designed. Superscript λ denotes the longitude and ϕ the latitude of the site's location. The sector boundaries are determined through the Voronoi decomposition of V.

Regarding weather disturbance and restricted airspace, unavailable airspaces are abstracted by their locations in a bounding circle. The location is taken as the latitude and longitude of their centers, and their shape as a circular bounding area. Even though weather regions are previously represented using grid-based and polygon-based shapes [13], the choice of circle is used here in order to maximize the area of available airspace around the periphery. The set of such disturbances is being denoted as D:

$$D = \{(\boldsymbol{d}_1, \mathrm{rad}_1), (\boldsymbol{d}_2, \mathrm{rad}_2), \ldots, (\boldsymbol{d}_\delta, \mathrm{rad}_\delta)\} \quad \text{where } \boldsymbol{d}_k = \begin{pmatrix} d_k^\lambda \\ d_k^\phi \end{pmatrix} \tag{2}$$

Here, $\boldsymbol{d}_k$ is the location of the disturbance center and rad_k is the radius of the circular bounding area. Note that δ is the total number of disturbances. It should also be noted that any arbitrary shape (represented by grid/polygon/circle) can be implemented in the CAARD algorithm with some modifications because the CAARD algorithm can simply avoid the placement of waypoints or routes in the hazard areas through the generation of new waypoints.

B. Traffic Flow Modeling

Regarding airways, the en route air traffic flow over Singapore is simulated based on the information derived from the Jeppesen charts of the Singapore FIR. The region considered is 0°N to 2.5°N and 102°E to 106°E. Major routes, also known as airways, have been identified as a sequence of waypoints (or fixes). These airways usually allow unidirectional flow and are vertically separated for traffic flowing in the opposite direction. In the current work, the airways that belong to a particular flight level with a constant unidirectional flow rate are simulated.

Let $A = \{a_1, a_2, \ldots, a_\alpha\}$ be the set of airways and each airway be represented as a sequence of waypoints:

$$a_i = (\boldsymbol{w}_{ij})_{j=1}^{\beta_i} \quad \text{where } \boldsymbol{w}_{ij} = \begin{pmatrix} w_{ij}^\lambda \\ w_{ij}^\phi \end{pmatrix} \tag{3}$$

Here, the number of airways is denoted as α and the number of waypoints that belong to a_i is denoted as β_i. The flow rate associated with a_i is denoted as f_i.

III. Simultaneous Optimization of Airway and Airspace

SAWAS is a framework developed in this paper to determine both an efficient sector and airway design that balances the workload distribution across sectors. An overview diagram of how the SAWAS

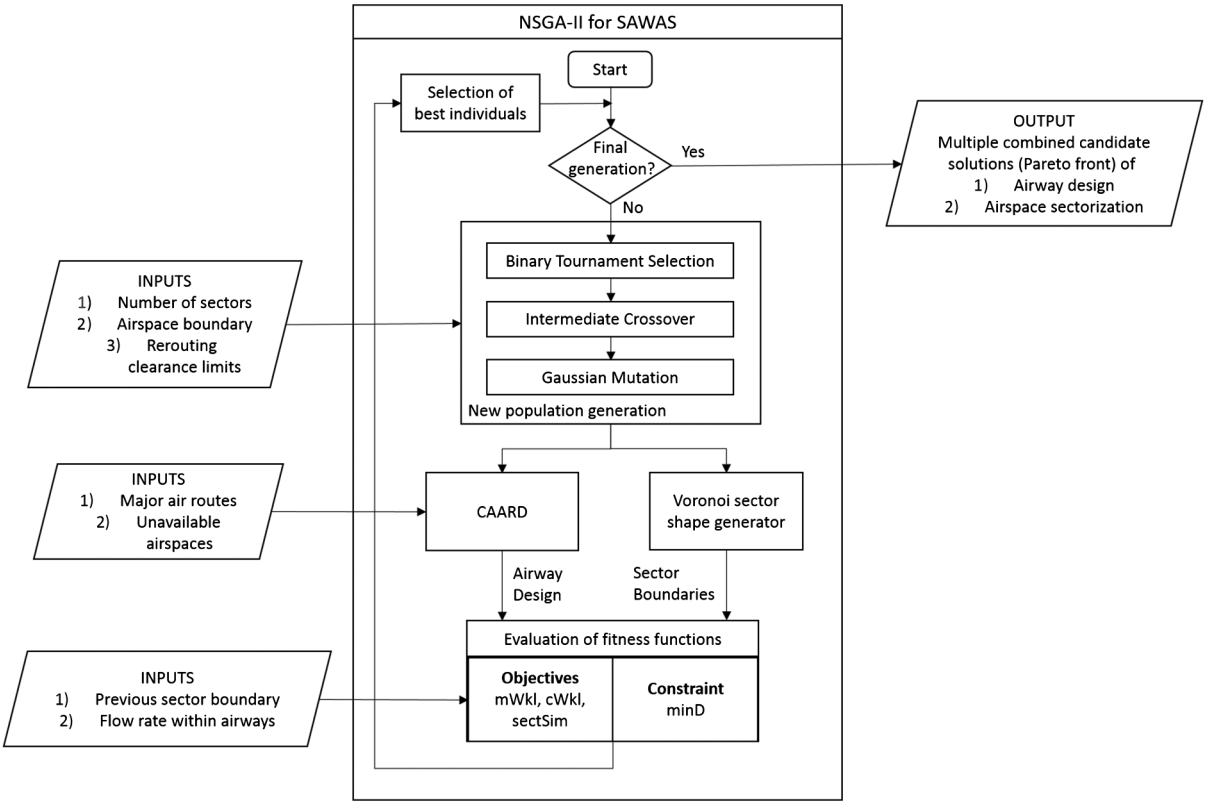

Fig. 3 Flow diagram for SAWAS.

framework is cast into NSGA-II (which stands for nondominated sorting genetic algorithm II) optimization is provided in Fig. 3. It depicts the parallel application of the CAARD algorithm for the airway design and the Voronoi sector shape generator for the airspace design. Using the flight plans and information on the unavailability of airspaces, multiple feasible airway designs are first generated using the CAARD algorithm. With one of the multiple airway designs and Voronoi sector shapes as inputs, the solution is evaluated using a multiobjective optimization model. These obtained objectives and constraints serve as feedback to the optimizer. The optimizer (NSGA-II) uses this feedback to improve the design through the variation of airway and Voronoi sectors until the termination condition is reached. The best design for the objectives is obtained as the output. The following subsections describe each of these subcomponents in more detail.

A. Airway Design Using CAARD Algorithm

With prior knowledge of the flight plans, the routes of individual flights may be designed so as to prevent congestion while also attempting to generate wind-optimal paths for fuel efficiency and avoids hazardous weather regions. The study of such convective weather, of its uncertainty [14] and impact [15], have been studied in recent years. Several works used weather prediction data and proposed techniques to generate alternate routes for the flows to avoid the weather impacted area as well to assure separation between flows. For example, Krozel et al. [16] found routes for individual flights, whereas Yang et al. [17] proposed the design of flexible airways in which separation assurance was left to the ATC. More recently, with the advancement of satellites, route planning could be improved in real time through the use of thunderstorm detection and nowcasting systems [18]. However, the impact of the rerouting on ATC workload has not been investigated in these works. In this paper, the reroute of airways to avoid constrained airspaces is based on flexible airway design. A novel path-planning algorithm is presented here, referred to as the CAARD algorithm. The foundation of the CAARD algorithm draws its inspiration from the A^* path-planning algorithm [19] that leverages upon classic Dijkstra's shortest path (that guarantees optimal solution) and greedy breadth-first-search (that provides faster solutions using heuristics) algorithms.

The airways are modeled as a sequence of waypoints or fixes in the CAARD algorithm. This allows for more complex airway designs, with flows that are convergent, divergent, or parallel and not necessarily monotonic, as assumed in [17]. Furthermore, it has been developed by giving consideration to certain specific requirements for incorporating it into the simultaneous optimization framework of SAWAS. The basic elements of the CAARD algorithm (viz., search space discretization, airway prioritization, and design of individual airways) are elaborated on in the following.

1. *Search Space Discretization*

The lateral separation criteria for aircraft is 5 n miles. To have a granularity higher than this, the airspace is divided into regular square grids of side lengths of 2 n miles. These grids are used to discretize the search space. A connected graph of finite nodes is constructed from these grids. The connectivity of the grids is based upon the possibility of intergrid traversal. The four cardinal directions [North (N), South (S), East (E), and West (W)] and the four intercardinal directions (NE, NW, SE, and SW) are taken as the eight possible directions of traversal from one grid to another.

The airspace is divided into γ unit grids, and $N = \{\boldsymbol{n}_1, \boldsymbol{n}_2, \ldots, \boldsymbol{n}_\gamma\}$ is the set of all grids. The individual grids are represented by the location of their centers as

$$\boldsymbol{n}_i = \begin{pmatrix} n_i^\lambda \\ n_i^\phi \end{pmatrix} \quad \text{for } i = 1, \ldots, \gamma \tag{4}$$

2. *Airway Prioritization*

The design problem of the CAARD algorithm involves path planning for multiple airways. In this work, the path planning is done sequentially by designing the first airway independent of others,

followed by the rest. Each subsequent airway attempts to avoid the set of all the previously designed airways. The sequence in which the airways are designed can influence the optimality of the final solution. Hence, the CAARD algorithm preprocesses the major routes to determine the degree to which each route is affected by the unavailable airspace. Airways that are most affected are assigned higher priorities and are routed first. Contrary to this approach, if unaffected airways are to be designed first, the flexibility in the design of the affected airway will be compromised. However, one may explore alternative approaches of prioritization to suit other requirements.

3. *Individual Airway Design*

The design of individual airways consists of two steps. The first step is to find the feasible waypoints for the given airway, avoiding all unavailable airspaces. The second step is to generate the route between these waypoints, maintaining sufficient clearances from other airways that have already been designed.

a. Generating Feasible Waypoints. To avoid unnecessary path planning, a line-of-sight check is performed between the waypoint pairs belonging to a particular airway. This helps to predetermine the presence of disturbances (untraversable airspaces) in the route. Supposing that the straight-line path between the waypoints w_{ij} and $w_{i,(j+1)}$ is obstructed, a simple geometric construction is done to stretch the path and avoid the disturbance by introducing a new waypoint w'_{ij}, as illustrated in Fig. 4a. The location of this waypoint is determined by the vector from the center of the disturbance, orthogonal to the line segment joining the waypoints w_{ij} and $w_{i,(j+1)}$. The length of this vector is determined by the optimization algorithm. This length could be chosen such that it is just sufficient to clear the obstruction. However, a higher clearance may be desired if it helps to balance the ATC's workload. Furthermore, the two possible directions of this vector become another variable, which is the same as allowing for positive and negative vector lengths. The variable length (and direction) of this vector allows for the much needed ability to generate multiple solutions from the path-planning algorithm. In the experimental studies, the length is chosen such that it is just sufficient to clear the obstruction with the direction varied, giving us a total of 2 × the number of affected routes permutations of rerouting strategies.

The clearance an airway needs to maintain from the unavailable airspace is represented by matrix C, which is given by

$$C = \begin{bmatrix} c_{11} & c_{12} & \dots & c_{1\delta} \\ \vdots & \vdots & \ddots & \vdots \\ c_{\alpha 1} & c_{\alpha 2} & \dots & c_{\alpha\delta} \end{bmatrix} \tag{5}$$

where $c_{ik} = |w'_{ij} - d_k|$, computed for $i = 1, \dots, \alpha$ and $k = 1, \dots, \delta$. The index j is based on the waypoint of a_i that is closest to d_k, along the direction of the traffic flow.

After determining the new waypoint, the routing can be updated from $(w_{ij} \rightarrow w_{i,(j+1)})$ to $(w_{ij} \rightarrow w'_{ij} \rightarrow w_{i,(j+1)})$. However, the disturbance may reside very close to or even encompassing the destination waypoint $w_{i,(j+1)}$. In this case, one needs to skip $w_{i,(j+1)}$ and route to the subsequent waypoint. Following this, a check is performed to ensure that the newly constructed path is unobstructed. The presence of multiple nearby disturbances might make the new waypoint infeasible, forcing one to iterate the aforementioned process for the new disturbance location. This is done until the new route is free of any disturbance. In Fig. 4b, this has been illustrated for the presence of two nearby disturbances. The airway a_i being designed is thus modified based on the feasible waypoints obtained and is denoted as a'_i. Once the feasible waypoints for an unobstructed path are obtained, the airway route between the waypoints can be generated.

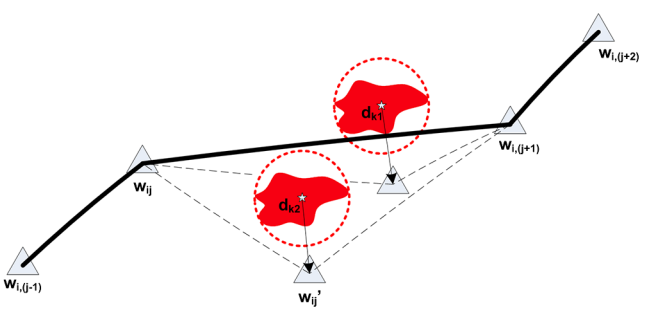

Fig. 4 Alternate waypoint generation in the presence of unavailable airspaces with multiple disturbances.

b. Routing of Airways. The waypoints obtained earlier only ensured traversable airspace in a straight-line path connecting these waypoints. However, it did not ensure a conflict-free path with other airways. Thus, it is necessary to determine if the straight-line path between these waypoints maintains sufficient clearances from other airways that were designed earlier. If so, a simple straight-line path between the waypoints can be incorporated into the current airway design. Otherwise, the path with least conflicts has to be determined. In a case of originally parallel flows, the newly designed airway needs to maintain a clearance from the previously (re)designed airways. For originally intersecting flows, orthogonal intersections are preferred in the redesign.

Path planning with these requirements is an optimization problem that needs to be solved by the CAARD algorithm. A separation clearance check, similar to the line-of-sight (LOS) check performed earlier, helps to reduce the scope of this optimization problem to only a select waypoint pairs. This helps to speed up the execution of the path-planning algorithm. Let r_i be the route of a_i that is currently being designed. This is nothing but a sequence of nodes (grids) $n \in N$. The set of all routes is denoted as R, and the set of previously designed airways is denoted as $\hat{R} \subset R$.

The path planning between the waypoints is cast as a cost minimization problem. In the context of the graph constructed by discretizing the airspace, this corresponds to finding the lowest-cost path from the source to the destination. The CAARD algorithm finds the sequence of nodes with the minimum cost of travel from the source to the destination waypoint. To determine this, it does not perform an exhaustive search among all possible options. Similar to A^* path planning, starting from the source, it preferentially expands the nodes that minimize the estimated cost of the total path to the destination. This is done by maintaining a list of nodes (FRONT) that are potential candidates for expansion. The preferential node n_{cur} for expansion at each stage is formulated as

$$n_{\text{cur}} = \arg\min_{n \in \text{FRONT}} (g(n) + h(n) + f_o(n) + \epsilon_1 f_c(\hat{R}, n) + \epsilon_2 f_{\text{LOS}-D}(n)) \tag{6}$$

Here, $g(n)$ is the distance cost from the node n to the source node. Note that $h(n)$ is the estimated distance (heuristic) from node n to the destination node. This heuristic distance is computed as the shortest diagonal distance (distance while traveling along the eight permissible directions) from node n to the destination node. This distance is only an estimate because there is no guarantee that this direct path is unobstructed. Also, $f_o(n)$ is the cost due to the presence of an unavailable airspace encompassing node n. Because paths that pass through unavailable airspaces are not permitted, this cost is infinity for such nodes and zero for the rest. Note that $f_c(\hat{R}, n)$ is the cost due to the presence of a previously designed airway within a specified clearance distance threshold from node n. Also, ϵ_1 is a scaling factor associated with this cost. $f_{\text{LOS}-D}(n)$ is the perpendicular distance from node n to the line segment connecting the source and destination waypoints. In other words, this is the cost of deviating from the straight-line path connecting the waypoints. This is added as a small perturbation cost to prefer straighter paths. Note that ϵ_2 is a scaling factor associated with this cost. During the process of graph exploration, the parent node of every explored

node is stored in order to trace back the shortest path from the source. The search stops once the destination node is reached through expansion.

B. Multiobjective Optimization Model: Objectives and Constraints

The objectives in the design of sectors and airways are directed at balancing the ATC workloads across all sectors, as well as at designing sector shapes that do not change drastically from the original sectorization. Furthermore, constraints are incorporated to obtain realizable sectors.

1. Objectives

The frequently used metrics to quantify the workload of ATCs include monitoring workload (representative of the number of aircraft monitored within a sector in a given time) and coordination workload (representative of the number of aircraft handed over to an adjacent sector in a given time) [20]. Other metrics like conflict workload (number of potential conflicts to resolve within the sector) [21] and dynamic density (a weighted average of heading change, speed change, etc.) [22] have also been used. In this paper, monitoring and coordination workload have been used as metrics for quantifying workload. However, the formulation considers individual flight trajectories and not airways; the metrics have been redefined here as follows:

1) The first metric is monitoring workload. This metric is used to evaluate the ATC workload in a particular sector owing to the presence of flights within that sector. In this paper, a constant rate of flights in each airway has been assumed. Thus, the time required to monitor a particular airway is proportional to the length of the airway within that sector as well as the rate of flights within that airway. Hence, the monitoring workload $mWkl$ of sector s_i is defined as

$$mWkl(s_i) = \sum_{m=1}^{\alpha} (\text{length of } a_m \text{ within } s_i) * (f_m) \tag{7}$$

2) The second metric is the coordination workload. This metric is used to calculate the number of handshakes between ATCs of adjacent sectors while transferring control of flights transitioning from one sector to the other. The coordination workload of a particular sector is proportional to the number of airways that have their flows exiting that sector, as well as to the flow rate within each airway. Thus, the coordination workload $cWkl$ is defined as

$$cWkl(s_i) = \sum_{m=1}^{\alpha} (\theta_m) * (f_m) \tag{8}$$

where $\theta_m = 1$ if a_m is an outgoing flow for s_i. Otherwise, it is zero.

3) The third metric is sector similarity. Dynamic airspace sectorization involves periodic reconfiguration of sector shapes in order to deal with changing traffic patterns and unavailable airspaces. Because this is the aim of the current work, the sector shapes should be disallowed to change drastically from the previous, thus allowing the ATC to monitor a region close to their area of specialization. Sector similarity is the metric used to calculate how similar a sectorization solution is to the original sectorization. A simple methodology for finding the 2-D shape similarity has been proposed in [23]. For every sector, the maximum overlapping area with all previous sectors is first computed. The ratio between this overlapping area and the original sector's area is used as the similarity metric for the corresponding sector. However, there is no mention of methodology to ensure that the same parent (old) sector is not mapped to two children (new) sectors.

To address this issue, a one-to-one parent–child relationship between the old and new sectors needs to be established before finding the sector similarity. This relationship is found by treating the mapping as an assignment problem where one needs to maximize the sum of similarity ratios of all sectors. The assignment is found by using integer linear programming with the constraint that every old sector is mapped to only one new sector. It is formulated as follows:
Maximum:

$$\sum_{i=1}^{\eta} \sum_{j=1}^{\eta} (\text{cor}_{ij} * x_{ij})$$

subject to

$$\sum_{i=1}^{\eta} (x_{ij}) \le 1 \quad \forall\ j$$

$$\sum_{j=1}^{\eta} (x_{ij}) \le 1 \quad \forall\ i$$

and

$$x_{ij} \in \{0, 1\}$$

Here, i is the index of old sector and j is the index of the new sector. Note that cor_{ij} is the similarity ratio between sector i and sector j. Also, x is the design variable where $x_{ij} = 1$ implies sector i is mapped as the parent of sector j. The values found would reflect the familiarity of the ATCs with the new sectors based on the mapping, and it provides a more accurate formulation of sector similarity and is denoted as $\text{sectSim}(s_i)$.

2. Constraints

The key features that are required for the designed sector shapes are incorporated as constraints of the optimization, and it includes the following:

1) The first features include convexity and connectivity. The internal angles of the sector shape must be less than 180 deg to avoid reentries and short dwell times for aircraft. Also, one sector must not be contained completely within another sector. Voronoi diagrams satisfy both these requirements. Because the sector shapes in this paper are found through Voronoi diagrams, no explicit convexity or connectivity constraint is imposed.

1) The second feature is the minimum distance from crossing points. Crossing points are points of intersection between major traffic flows, and they are critical areas monitored by ATCs. Such regions need to be sufficiently far from sector boundaries to provide higher response times to the ATC for ensuring the safety of operations. In this paper, the intersection points between the designed airways are determined and denoted as cp_i for i ranging from $(1, \ldots, \psi)$. Note that ψ is the total number of crossing points found for a given air traffic flow. A constraint is imposed to ensure the crossing points are at least 10 n miles from the nearest sector boundary.

The minimum distance metric is formulated as

$$\min D = \min_{i=1}^{\psi} \|\text{cp}_i, \text{boundaries}(s_m)\| \tag{9}$$

where $\text{cp}_i \in s_m$. The constraint can be written as $\min D < 10$ n miles.

C. NSGA-II Optimization

A variety of mathematical techniques have been employed in the literature to compute optimal sector shapes that balance ATC workloads across given sectors. This includes constraint programming, evolutionary optimization, mathematical programming, stochastic local search, and spectral clustering, among others [20]. Most of these algorithms do not resort to performing an exhaustive search but rather use heuristics to

obtain near-optimal solutions. The optimization problem in this paper can be expressed as follows:

Find: The Voronoi sites and the clearance matrix $[V, C]$
Subject to:
Objectives:
1) Minimize the deviation of monitoring workloads across sectors.
2) Minimize the sum of coordination workloads of all sectors.
3) Maximize the average sector similarity with the original sectors.
Constraint:
1) Maintain a minimum distance of 10 n miles from all crossing points to their nearest sector boundaries.
Bounds:
1) $\min \text{Lat} \leq v_i^{\phi} \leq \max \text{Lat}$ AND $\min \text{Lon} \leq v_i^{\lambda} \leq \max \text{Lon}, \forall\ v_i \in V$
2) $-\text{maxClearance} \leq c_{ik} \leq -\text{minClearance}$ OR
$\text{minClearance} \leq c_{ik} \leq \text{maxClearance}, \forall\ c_{ik} \in C$

This problem is a multiobjective, constrained optimization with a large decision space $(2 * \eta + \alpha * \delta)$. In this paper, the nondominated sorting genetic algorithm II [24] has been employed to solve this optimization problem. Also, multiobjective optimization produces multiple solutions (Pareto-optimal solutions) that vary in the tradeoffs between specified objectives. This will provide options for the ATCC manager to select the best-suited solution for a given scenario.

NSGA-II uses nondominated sorting to reduce the computational complexity and a crowding distance metric to increase the diversity of solutions. It also defines a constrained-domination principle to handle the constraints specified. The ranking of solutions is first based on feasibility using constraint violation. Feasible solutions are further subdivided into sets of nondomination, which are internally ranked based on the crowding distance metric. The set of infeasible solutions is then ranked based on the value of constraint violation.

IV. Performance Evaluation of SAWAS

In the previous section, the SAWAS framework for performing a concurrent optimization of airway and sector design was presented. In this section, the performance evaluation of SAWAS is given in two experimental studies. The first study is in a simulated environment described to highlight its working and its benefits. This second study is implemented using the Singapore FIR to show it is working in a real-life scenario.

A. Simultaneous Versus Sequential Approach

For this study, the three major airways in Singapore's en route airspace (as in Fig. 2) were chosen for the simulation. The air traffic within these airway routes was simulated, assuming equal flow rates of 10, for a 2 h time window. First, a strategic sectorization using these flight data was performed to serve as a basis for comparison. Subsequently, the study was done under a pretactical stage where a section of airspace was made unavailable, requiring rerouting. For this scenario, the performance comparison of a sequential solution with the proposed simultaneous solution (by SAWAS) for the airway and sector design is presented.

1. *Strategic Sectorization*

Strategic sector design is a decision-making process for synthesizing efficient sectors, a day to a week in advance, for a given flight plan. To find the efficient strategic sector design, NSGA-II optimization is used, using the framework elaborated in Sec. III. However, because the entire airspace is considered available at the strategic stage, the CAARD algorithm does not play any role in this optimization. This optimization is performed with the monitoring and coordination workload objectives as well as a minimum distance constraint. The sector similarity objective is not included because, at the strategic stage, there is flexibility in the sector design and the aim is to find the best static solution for the given air traffic flow. For the software implementation of NSGA-II, NGPM v1.4 (which stands for NSGA-II program for MATLAB) [25] is used. The parameter settings are a population size of 50, maximum generations of 200, an immediate crossover ratio of 1.2, a Gaussian mutation scale of 0.1, and shrink of 0.5.

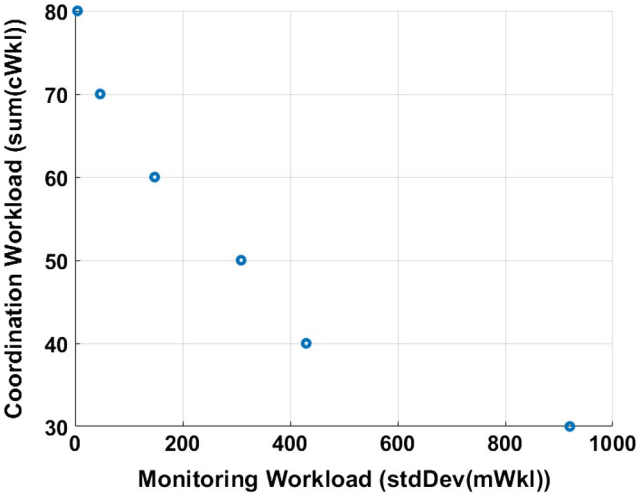

Fig. 5 Pareto front for strategic sectorization (stdDev denotes standard deviation).

Figure 5 shows the plot of few representative solutions on the obtained Pareto front. The variety of solutions presented here depicts the advantage of casting the design problem as a multiobjective optimization. Multiple solutions, with differing tradeoffs among objectives, are thus made available for the ATCC to evaluate based on their preferences.

The chosen strategic solution, along with a bar graph of the variation sectorization metrics, is shown in Fig. 6. The bar graph shows an even distribution of monitoring workload across sectors with a standard deviation of 169. The coordination workload ranges from 0 to 20: the sum of which is 60. An alternate way to view this metric is as being proportional to the total number of outgoing airways that are cut by the sector boundaries (which in this case is six). With reference to Fig. 5, one can observe that the objectives of the chosen solution can be represented by the third solution from the left on the Pareto front.

2. *Pretactical Airway and Sector Design*

Having obtained the strategic sector shapes, a pretactical scenario is simulated in which an airspace along airway 1 was excluded, deeming it unavailable. In reality, this may be invoked by a military aviation authority or due to a weather forecast. The unavailability of airspace can be of any shape. In our experiments, this is modeled by a circle for convenience. One approach to design both airways and sectors for a given air traffic is to design them sequentially: the airway rerouting performed first, followed by the sector design for the newly generated airways. This approach has been used in [6], where such a sequential strategy has been proposed to handle this problem. In the following subsection, the results of this approach are first presented. In the subsequent subsection, these results are then compared with those obtained from a concurrent optimization by SAWAS.

a. Sequential Solution (Rerouting Followed by Resectorization). A sequential solution requires one to find feasible routes for flights before sectorization. Without changing the strategic sector shapes, the CAARD algorithm is used independently to find feasible routes. Two possible reroute strategies generated by the CAARD algorithm, where airway 1 maintains the minimum allowed clearance on either side of the unavailable airspace, are generated.

The bar graphs in Figs. 7a and 7b show the variation of sectorization metrics for the two reroute strategies (northward and southward, respectively) without any change in sector design. The visualizations of these two rerouting strategies, which we refer to as southward and northward, are shown in Figs. 8a and 9a, respectively. Comparing the two strategies in terms of these

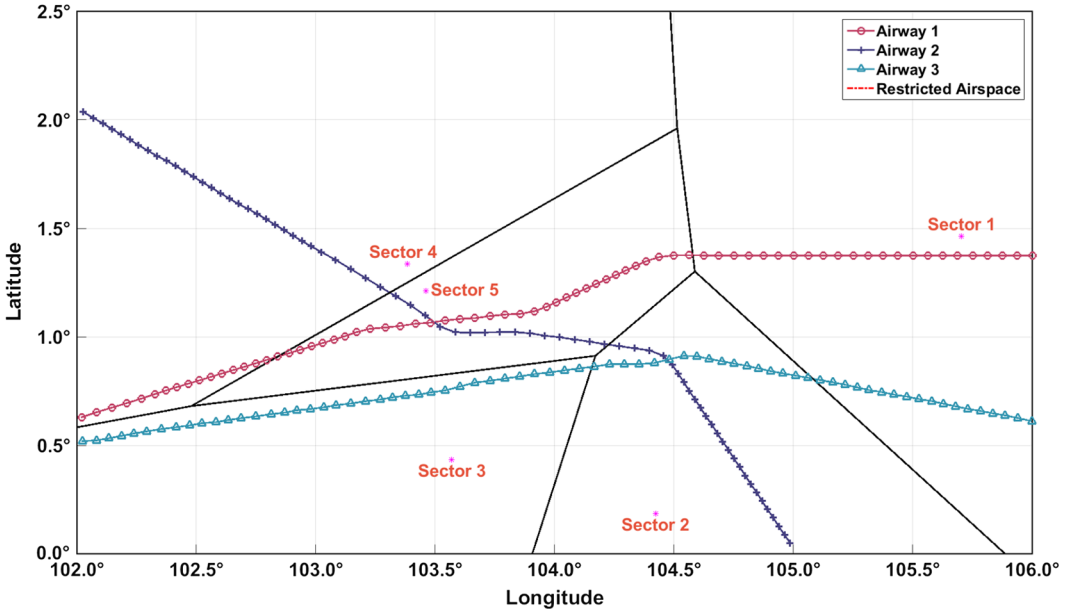

a) Visualization of sector shapes

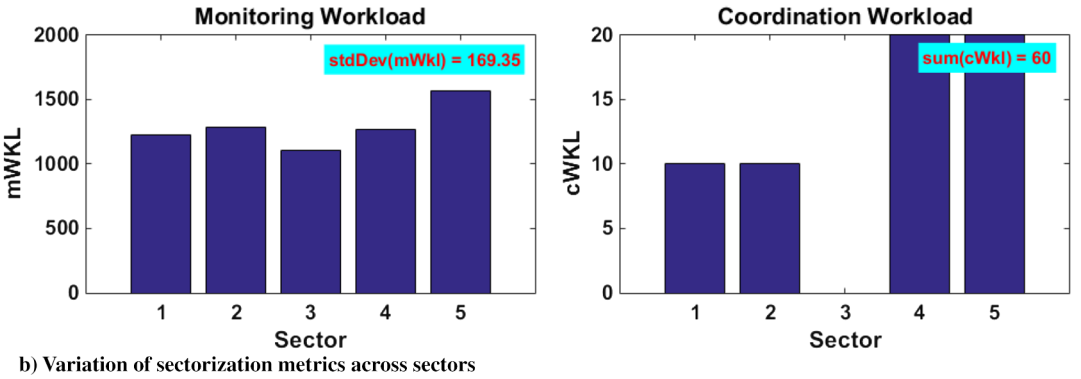

b) Variation of sectorization metrics across sectors

Fig. 6 Selected strategic sectorization solution and its objectives.

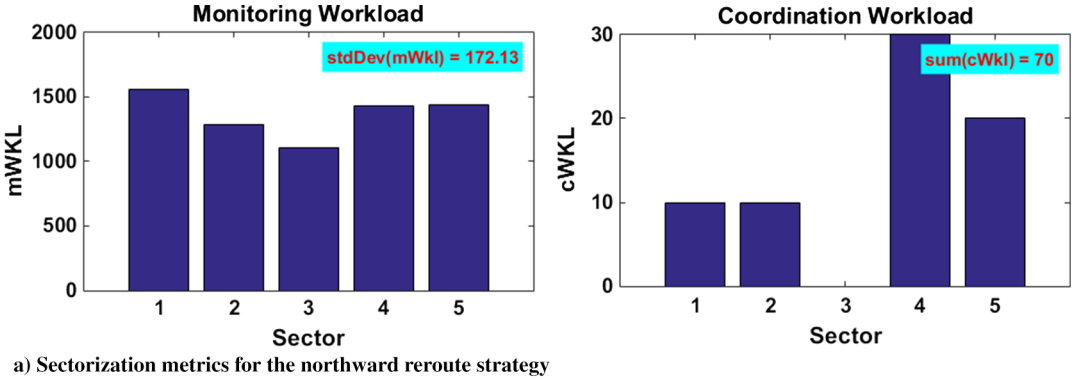

a) Sectorization metrics for the northward reroute strategy

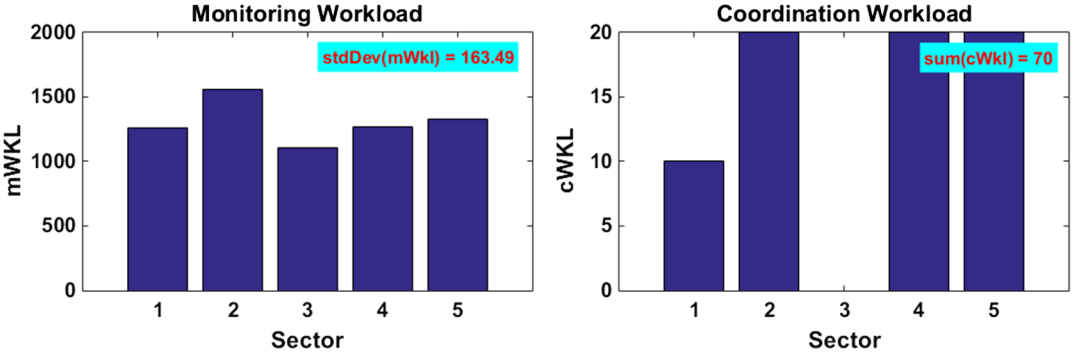

b) Sectorization metrics for the southward reroute strategy

Fig. 7 Variation of sectorization objectives across sectors for different reroute strategies.

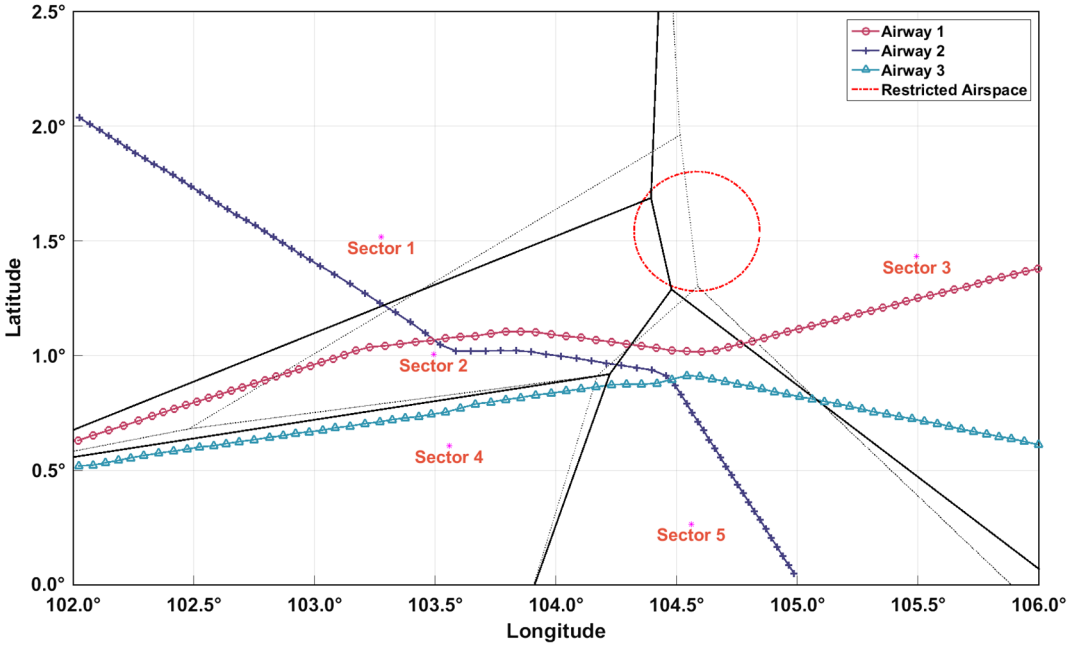

a) Visualization of sector shapes and southward rerouting (old sectors are indicated as dotted lines)

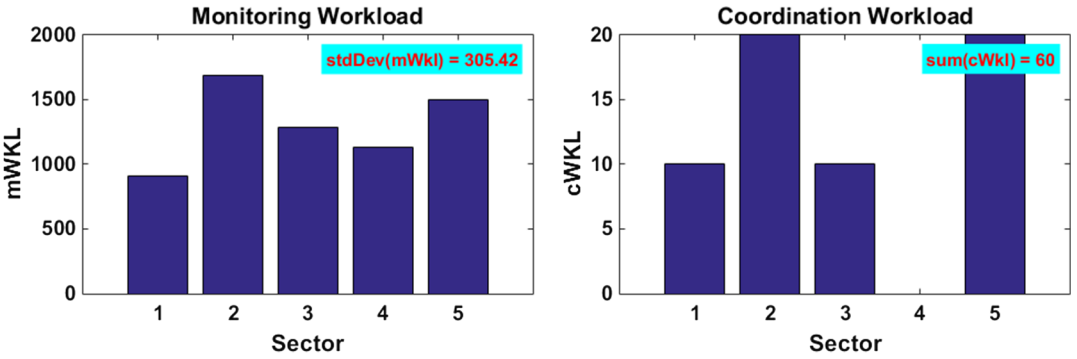

b) Variation of sectorization metrics across sectors

Fig. 8 Best sequential airway and sector design solution, and its performance metrics (rerouting followed by resectorization).

metrics, the southward reroute strategy has a lower monitoring workload variation (163 as opposed to 172). This is due to the fact that northward reroute strategy involves a longer path, and hence higher monitoring workload, for sectors 1 and 5. The sum of coordination workloads is the same for both strategies because they both involve an extra entry and exit into an adjacent sector. However, the range is higher for the former (0–30 as opposed to 0–20). The sector shapes being unchanged with respect to the strategic sectorization, the average sector similarity is 100% for both cases. To decide which strategy to use for the resectorization step, one can base the choice on the solution that performs better on the sectorization metrics. Based on the three metrics, the southward reroute strategy for airway 1 seems more attractive.

Next, an independent sector optimization was performed where the airway design was kept fixed. All three objectives were included in the optimization, where the sector similarity was evaluated with respect to the strategic sectorization. The minimum distance constraint was also imposed. The solution with a reasonable tradeoff between the objectives was chosen, for which the sector shapes are visualized in Fig. 8.

Figure 8a shows that the new sector design (black unbroken lines) is similar to that of the original strategic sectorization (light dotted lines). The bar graph in Fig. 8b shows the variation of sectorization metrics for this solution. Because airway 1 is rerouted south of the unavailable airspace, it passes close to the crossing flow of airways 2 and 3. Due to the minimum distance constraint, sectors 2 and 3 are unable to expand to take up their original flow passing through airway 1. This restricts the ability to redesign the sector to reduce the monitoring workload and creates a high standard deviation of 305. The only improvement possible through resectorization is the reduction in coordination workload of sector 1 through the expansion of sector 2 in the west. The total coordination workload is also reduced.

b. Concurrent Solution by SAWAS. SAWAS overcomes the aforementioned limitations of the sequential design approach, which involves intermediary decisions that tend to be greedy in nature. To illustrate this claim, the SAWAS architecture is used for optimizing both the airways and sector design concurrently. All three objectives are included in the optimization. The minimum distance constraint is also imposed. The solution with a reasonable tradeoff between the objectives is chosen, for which the sector shapes are visualized in Fig. 9a. The new sector shapes are reflected with black unbroken lines, and the previous sector design is shown with light dotted lines.

From Fig. 9a, it may be noted that the northward reroute strategy was preferred instead by the optimizer. The bar graph in Fig. 9b indicates an improvement in both monitoring workload imbalance (which is reduced to 132) and coordination workload sum (which is reduced to 60) post-resectorization. In this resectorization, sector 3 has expanded toward sector 1 in the northern airspace to take up the redirected flow within airway 1. This reduces the extra coordination workload for sector 1. To prevent overloading of sector 3, sector 1 has expanded toward sector 3 in the western region, taking up additional control of airway 1. Consequently, a drop in sector similarity is noted for sectors 1 and 3. Compared to the sequential solution that could only improve the coordination workload, the SAWAS solution was

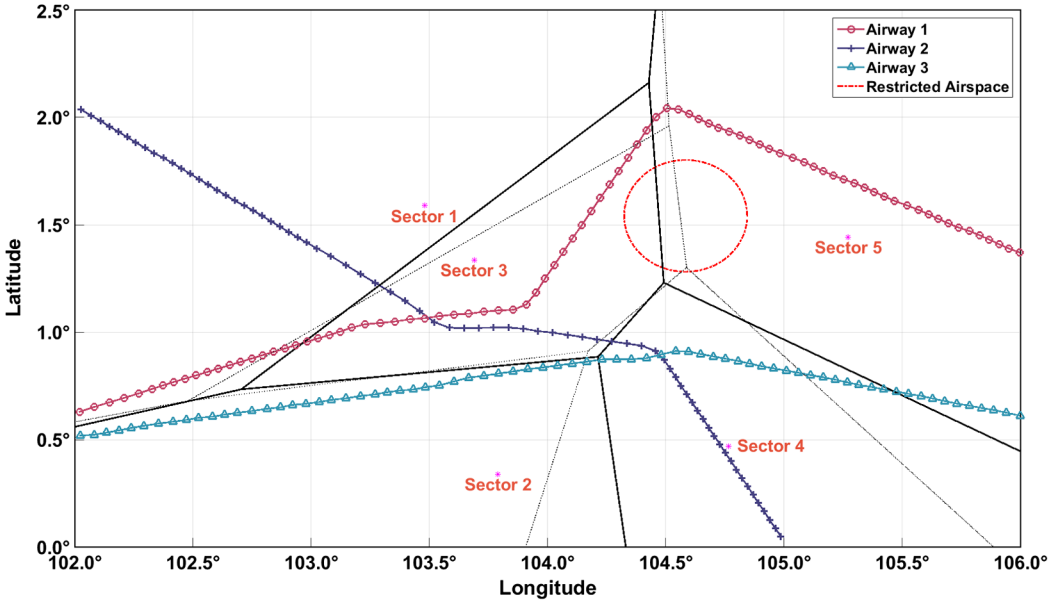

a) Visualization of sector shapes and northward rerouting (old sectors are indicated as dotted lines)

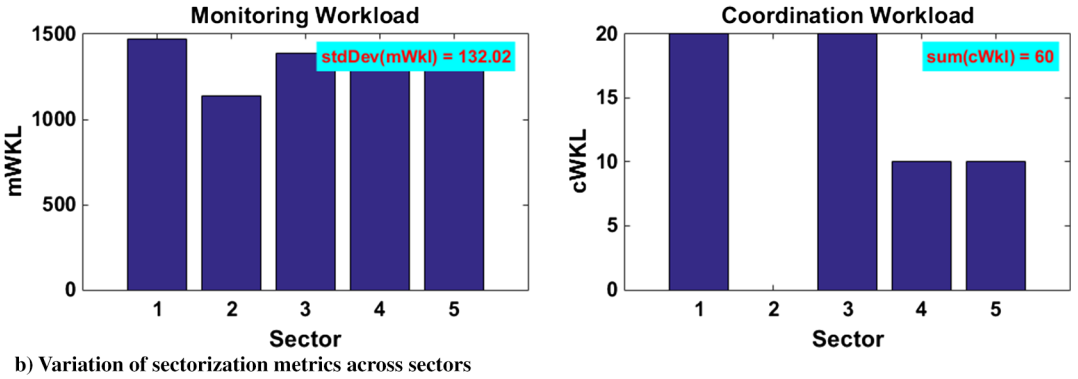

b) Variation of sectorization metrics across sectors

Fig. 9 Best SAWAS airway and sector design, and its performance metrics.

able to achieve an improvement in both monitoring as well as coordination workloads. Both sequential and SAWAS solutions maintain a high sector similarity above 85%.

Although the northward redirection of airway 1 yields unoptimal fitness function values for the strategic sector shapes, it yields a more optimal solution after resectorization. The sequential approach requires the assumption that an optimal airway design will yield an overall optimal solution. SAWAS, on the other hand, concurrently considers the effect that resectorization and rerouting have on the objectives. It evaluates which combined strategy is best suited for the objectives. Thus, SAWAS manages to outperform the sequential approach.

SAWAS is envisioned to serve as a decision support tool for ATCCs for pretactical decision making, incorporating considerations of dynamic weather conditions and airspace availability. The optimal sector and airway redesign found at the pretactical stage could feed as input to the ATCC for this decision making. ATCs would have to change their area of control and convey reroute instructions to redirect the flights in the affected airways.

B. Performance Evaluation of SAWAS on Singapore FIR

The airways used in this experiment were under Singapore air traffic control in the upper airspace (above flight level 135) of the Singapore FIR. There was a total of 27 flight routes (airways), which were extracted from the Civil Aviation Authority of Singapore's Aeronautical Information Publication.[¶] Next, the flow rates of the airways were estimated using the historical flight data recorded on 1 June 2015.[**] The flight data consisted of automatic dependent surveillance broadcast (ADS-B) data with two to four positions per minute, depending on coverage of area and air navigation service provider (ANSP) radar from governments that were about one position per minute. However, the provided tracks only covered up to 108 in longitude, which did not cover the whole Singapore FIR. Therefore, flight data from the longitude of 108 to 116.3 were extrapolated from the provided flight plans. The flow rates were then obtained through matching the combined set of flight tracks to the airways using waypoints. It was also worth noting that, by this approach, approximately 70% of flights were captured; hence, these rates might be slightly lower than the actual rates. The total flow rates varied significantly throughout the day. Furthermore, the flow rates for each airway changed almost every hour, and not all airways were used at all time. Thus, it can be said that air traffic varied throughout the day and resectorization was required to balance the workloads. For this particular experiment, we took 1 h worth of flights when the flow rates were heaviest from 1600 to 1700 hrs. This covered the use of 20 airways with varying flow rates.

1. *Strategic Sectorization*

This section provides the results for sectorization with the assumption of no weather disturbances. Similar parameter settings for NGPM NSGA-II optimization as in Sec. IV.A are selected, with

[¶]"Aeronautical Information Publication (AIP)," Civil Aviation Authority of Singapore, data available online at https://www.caas.gov.sg/docs/default-source/pdf/amdt.pdf.

[**]"Flight Data in Singapore Regional Airspace in June 2015," FlightAware, www.flightaware.com.

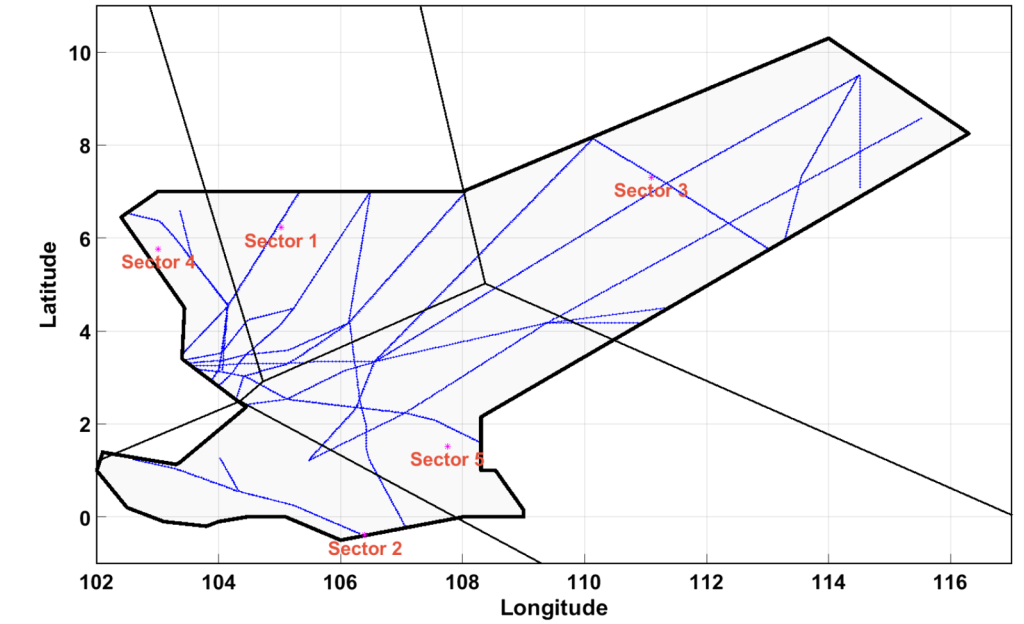

a) Visualization of sector shapes

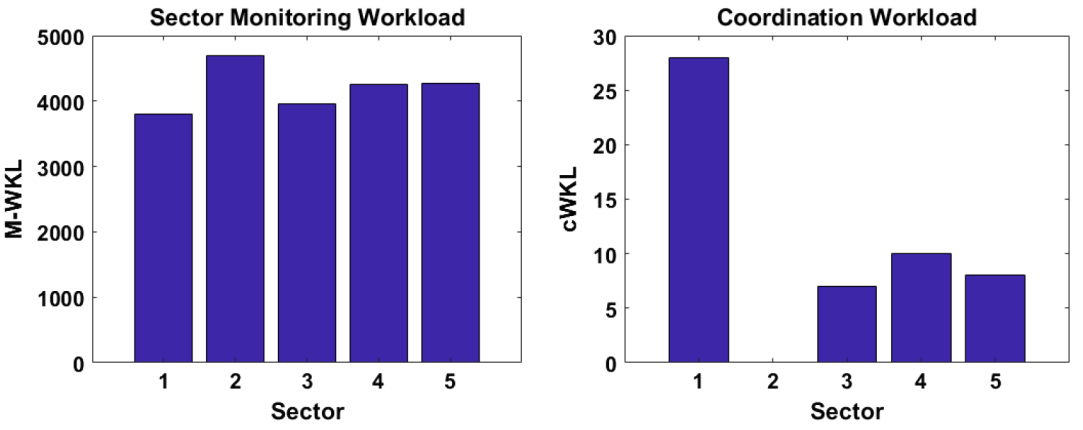

b) Variation of sectorization metrics across sectors

Fig. 10 Selected (solution A) sectorization for Singapore FIR.

an exception for the choice of the maximum generations of 500 due to a larger number of airways and varying flow rates.

Due to the unique and nonconvex shape of the Singapore FIR, the boundaries of the airspace are no longer a box but polygon shaped like the Singapore FIR. Furthermore, the generated Voronoi sites must lie inside the Singapore FIR. Therefore, the convexity of the sector shape in this study cannot be guaranteed. Out of 50 solutions, a total of 27 solutions lies on the Pareto front. The standard deviation of monitoring workloads among all the sectors for all Pareto-optimal solutions ranges from 334 to 6643. However, the huge imbalance of monitoring workloads among sectors is not preferable because it could reflect having empty sector(s) at the expense of overloading other sectors. Therefore, it is in our interest to focus on the solutions with a low standard deviation of monitoring workload on the Pareto front.

Figure 10 provides the selected solution A with the monitoring and coordination workloads of the sectors. The blue lines in Fig. 10a represents all considered routes in the Singapore FIR (shape outlined in bold black), and the black lines represent the sector design. Each sector is the overlapping area between the sector design and the Singapore FIR. Figure 10b shows that the monitoring workload is well balanced among all five sectors between 3500 to 5000, with a standard deviation of 343. The coordination workload of sectors ranges from 0 to 28, giving a total of 53 among all sectors. Similar to the previous experiment (in Sec. IV.A), this solution acts as a baseline. Looking at Fig. 10a, sector 4 has a small separate airspace that is connected to sector 2. This is the consequence of the nonconvexity constraint not being met. In this case, a postprocessing of assigning the small area of airspace from sector 4 to sector 2 is performed.

2. *Change in Airspace Availability*

In this section, a pretactical scenario where a particular airspace becomes unavailable is provided. In this given scenario, two airways are being affected by the unavailability of this airspace. A rerouting of the affected airways is first performed using the CAARD algorithm. A total of 2^n possible rerouting strategies will be generated, where n represents the number of affected airways. In this case, a total of four ($2^2 = 4$) possible reroute strategies is generated. Figure 11 shows the initial affected routes with four possible reroute strategies generated by the CAARD algorithm. Table 1 shows the corresponding performance objectives and characteristics of the rerouted solutions. Overall, the monitoring workload among all sectors becomes more imbalanced, with the standard deviation increasing from 343 to 600–800. The coordination workload increases for solutions A1, A2, and A4, but it decreases by one for solution A3. Furthermore, the safety constraint of minimum distance to crossing points has to be checked. The rerouting of solution A2 in Fig. 11c and A4 in Fig. 11e

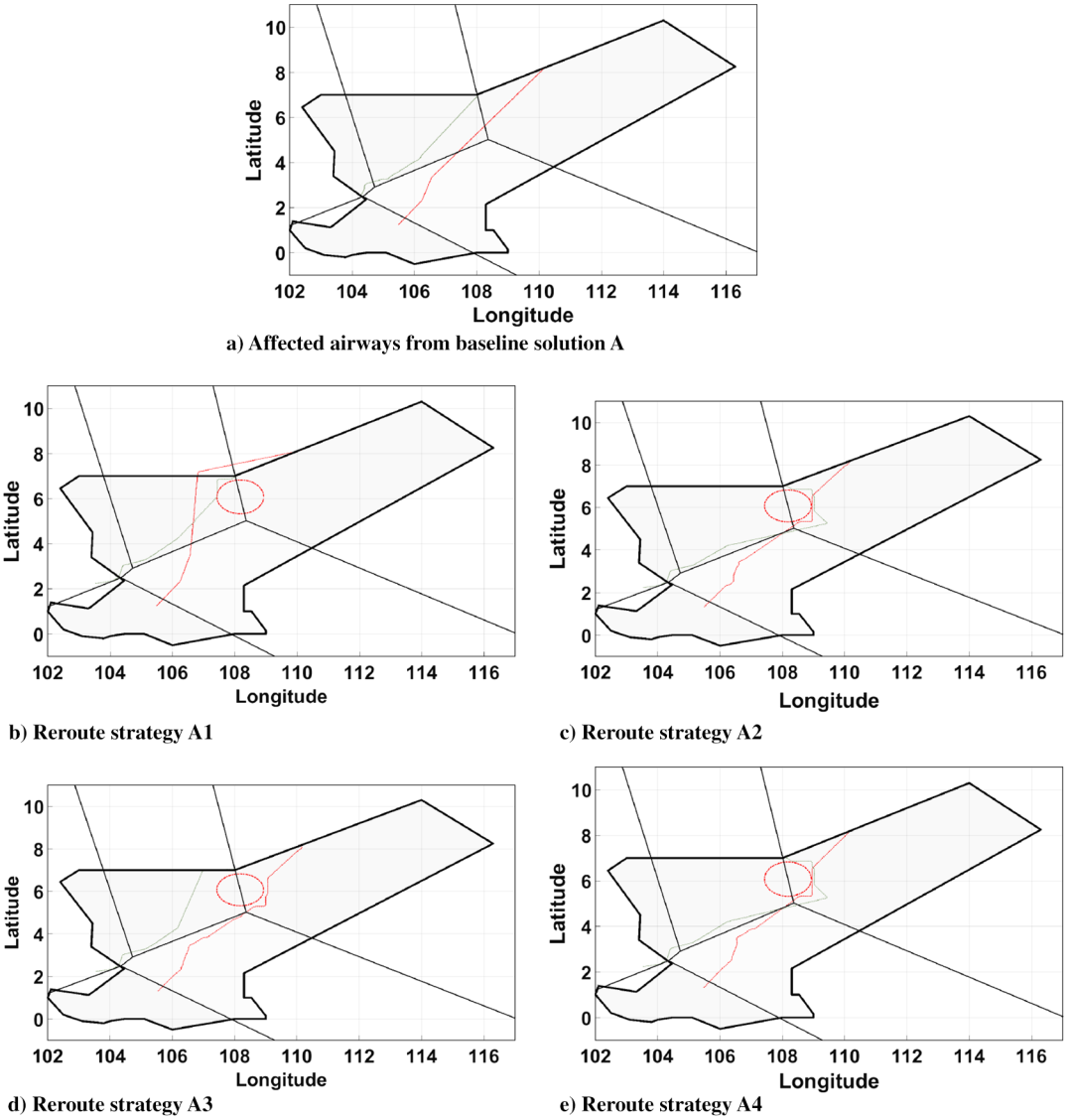

a) Affected airways from baseline solution A

b) Reroute strategy A1

c) Reroute strategy A2

d) Reroute strategy A3

e) Reroute strategy A4

Fig. 11 Affected routes and possible reroute strategies generated by the CAARD algorithm.

displays a crossing point very close to the sector boundary between sectors 1 and 5, hence not satisfying the safety constraint. Last, but not least, the route feasibility of the solutions has to be checked. Visually, we can observe that the rerouted solution A1 in Fig. 11b is infeasible because part of airway 2 is out of the Singapore FIR. One should note that this occurrence is because of the nonconvex shape of the Singapore FIR. Given a convex airspace, this situation is unlikely to happen. Also, it can be seen that solutions A2 in Fig. 11c and A4 in Fig. 11e are similar to each other. This similarity in routes is also reflected in their closely matched performance objectives in Table 1. With this, the only feasible solution without any resectorization is solution A3 in Fig. 11d.

Figure 12 provides solution A3 and its sectorization metrics across all sectors. The red lines represent airways that have been rerouted.

Table 1 Performance characteristics of the CAARD algorithm solution

Route	stdDev(mWKL)	sum(cWKL)	Constraint	Feasibility
A1	789.5	56	Yes	No
A2	688.3	55	No	Yes
A3	773.0	52	Yes	Yes
A4	663.4	55	No	Yes

The monitoring workloads range between 2500 to 5000 with a standard deviation of 773. The coordination workloads range from 0 to 27, giving a sum of 52. The sectors remained unchanged, thus 100% similarity score were obtained for all sectors.

To get more balanced monitoring workloads, we perform SAWAS on the current scenario using feasible rerouting strategies A2, A3, and A4 in Fig. 11 with a maximum generation of 2000. The number of generations is being increased here again to capture the possible variation of new rerouting strategies, which was not present in strategic sectorization.

Figure 13 displays the performance objectives of 50 Pareto-optimal solutions obtained using SAWAS (designated with circles) and four solutions only rerouting A1, A2, A3, and A4 (designated with plus signs). The x axis and y axis represent the standard deviation of the monitoring workload and the total coordination workload among all sectors, respectively. This range of solutions obtained by SAWAS presents the user with more permutations of rerouting and resectorization as compared to performing a rerouting followed by resectorization after choosing a set of particular routes. Figure 13 shows how solution P dominates solutions A1, A2, and A4 but is incomparable to solution A3 in terms of the performance objectives. This allows us to conclude that solution A3 is a good choice of solution, should the user decide that sectors are to remain unchanged. Next, we present a solution with a more balanced monitoring workload among sectors (lower standard deviation of

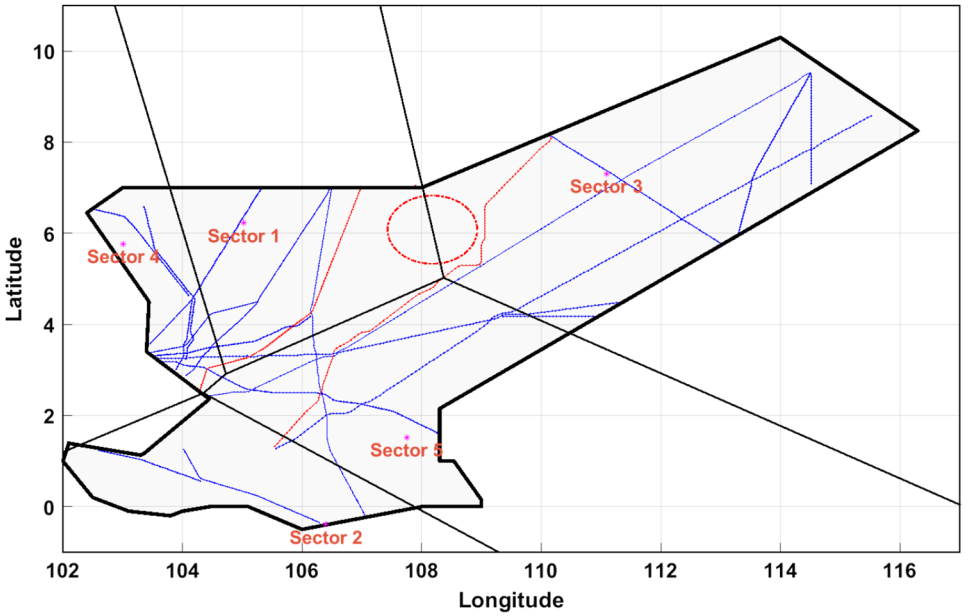

a) Visualization of sector shapes

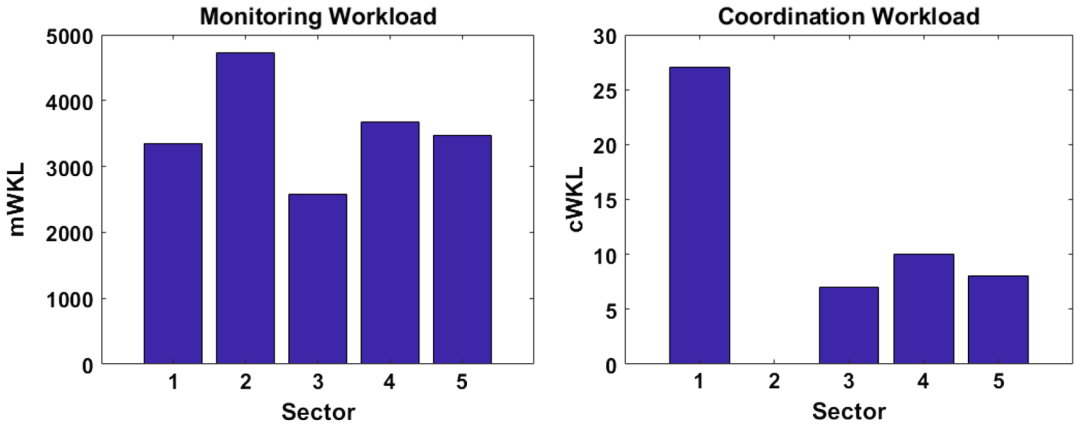

b) Variation of sectorization metrics across sectors

Fig. 12 Solution A3 (rerouting solution without resectorization).

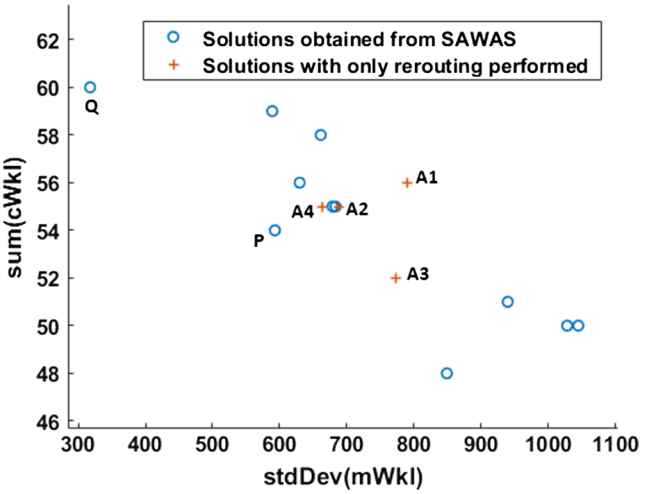

Fig. 13 Pareto front obtained using NSGA-II with restricted airspace.

monitoring workload): solution Q. In comparison with solution P, it can be said that solution Q has gained a larger coordination workload as a tradeoff for better balance of monitoring workload between sectors.

Figure 14 displays the sectors in solution Q (a solution that has 318 as the standard deviation of monitoring workloads among sectors), which is similar to that of the original sectorization. This is reflected in Fig. 14b, where the sector monitoring workload is much more balanced as compared to solution A3 in Fig. 12b. Again, solution Q is using the same set of routes as solution A4. The affected routes for rerouting are represented with red lines in Fig. 14a (same as reroute strategy A4 in Fig. 11e), and the blue lines represent the other unaffected routes. In this case, the coordination workload ranges from 0 to 31 and the total incurred is 60. The sector similarity to solution A is 74%. This sector shape change is being visualized in Fig. 14a, where the black unbroken lines represent the new sector design and the light dotted lines show the initial sector design.

Ultimately, SAWAS provides the user more choices in the selection of solutions. Furthermore, just rerouting did not guarantee constraint satisfaction (e.g., safety constraint), whereas SAWAS gives solutions that guarantee this through consideration of the interactions between rerouting and sector geometry. If the user has a preference for balanced monitoring workloads among sectors, solution Q will be preferred. However, if the user prefers unchanged sectors, solution A3 will be chosen. The choice of sectors here will have an impact on the air traffic operations in the future. Therefore, the final choice of sectors should be determined with the use of information on predicted future air traffic.

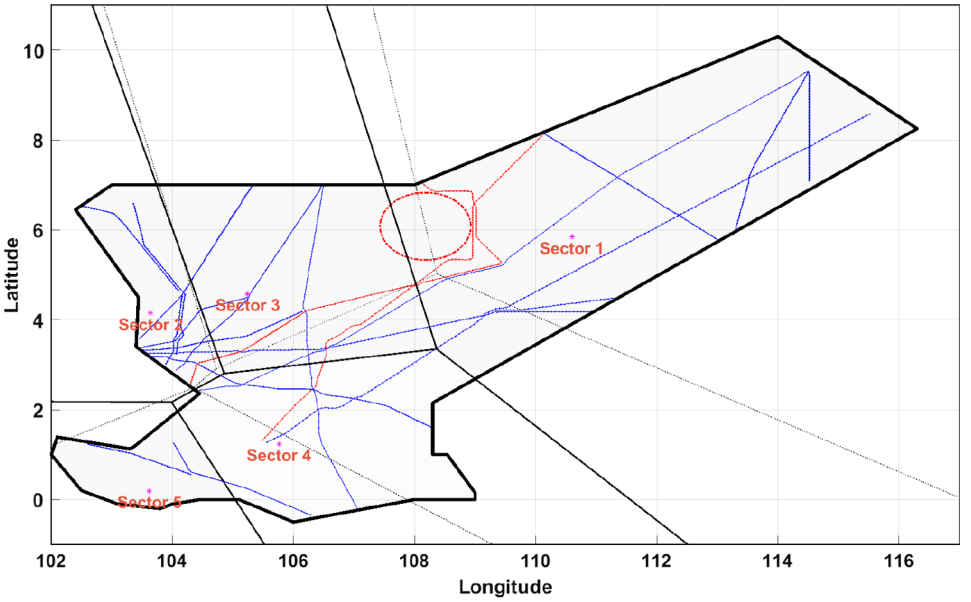

a) Visualization of sector shapes

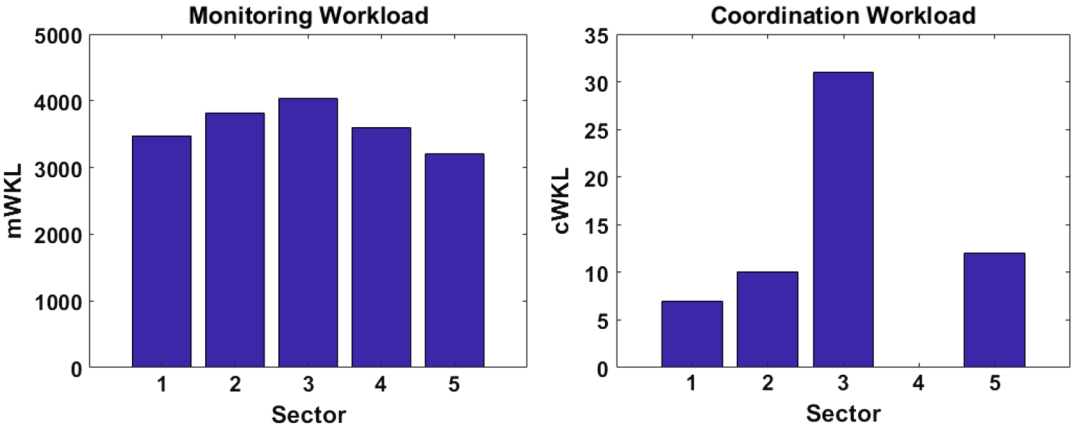

b) Variation of sectorization metrics across sectors

Fig. 14 Solution Q with better balancing of monitoring workloads.

V. Conclusions

In this work for the balancing of the ATC workload, a methodology to simultaneously use sector design and traffic routing as variables was explored. The proposed methodology consisted of three key components: airspace sector design, traffic flow design, and optimization. Voronoi diagrams were employed for the sector design. The traffic flow design had unique requirements to allow its usage as a design variable, such as the need to generate multiple solutions and to resolve conflicts between multiple airways. Thus, a novel algorithm was developed to satisfy these requirements. Multiobjective constrained optimization using an evolutionary algorithm was employed to find the optimal sector redesign and traffic reroute. To test the efficacy of the algorithm, a simulation environment was set up with synthetic air traffic and airspace disturbances in the context of Singapore air traffic control. A sequential strategy where the traffic flow design preceded the sector design was compared with the simultaneous optimization. In the sequential strategy, the traffic flow design lacked prior knowledge on future sector shapes. Hence, it required the assumption that optimal traffic flow design would lead to an overall optimal solution for the design objectives. The current solution overcame this shortcoming by concurrently considering the effect of the sector and flow redesign on the objectives.

Acknowledgments

The authors wish to thank the reviewers for their insightful comments and extend their thanks to the Air Traffic Management Research Institute, Nanyang Technological University in Singapore (ATMRI:2014-R8), for providing financial support to conduct this study.

References

[1] "IATA Forecasts Passenger Demand to Double over 20 Years," International Air Transport Association Press Release No. 59, Oct. 2016, http://www.iata.org/pressroom/pr/Pages/2016-10-18-02.aspx [retrieved 2017].

[2] "Asia/Pacific Area Traffic Forecasts 2008–2025," Report of the Fourteenth Meeting of the Asia/Pacific Area Traffic Forecasting Group (APA TFG), International Civil Aviation Organization Doc. 9915, https://www.icao.int/sustainability/Documents/Doc9915_en.pdf [retrieved 2017].

[3] Yousefi, A., and Donohue, G., "Temporal and Spatial Distribution of Airspace Complexity for Air Traffic Controller Workload-Based Sectorization," *AIAA 4th ATIO Forum*, AIAA Paper 2004-6455, pp. 822–834. doi:10.2514/6.2004-6455

[4] Drew, M., "A Method of Optimally Combining Sectors," *9th AIAA ATIO Forum*, AIAA Paper 2009-7057, 2009. doi:10.2514/6.2009-7057

[5] Klein, A., Kavoussi, S., Lee, R., and Craun, C., "Estimating Avoidable Costs Due to Convective Weather Forecast Inaccuracy," *11th AIAA ATIO Conference*, AIAA Paper 2011-6811, 2011. doi:10.2514/6.2011-6811

[6] Klein, A., Lucic, P., Rodgers, M. D., Leiden, K., and Brinton, C., "Exploring Tactical Interaction Between Dynamic Airspace Configuration and Traffic Flow Management (DAC-TFM)," *IEEE/AIAA 31st Digital Avionics Systems Conference (DASC)*, IEEE Publ., Piscataway, NJ, 2012, pp. 4A1-1–4A1-13. doi:10.1109/DASC.2012.6382326

[7] Tang, J., Alam, S., Lokan, C., and Abbass, H. A., "A Multi-Objective Approach for Dynamic Airspace Sectorization Using Agent Based and Geometric Models," *Transportation Research Part C: Emerging Technologies*, Vol. 21, No. 1, April 2012, pp. 89–121. doi:10.1016/j.trc.2011.08.008

[8] Delahaye, D., Schoenauer, M., and Alliot, J. M., "Airspace Sectoring by Evolutionary Computation," *IEEE World Congress on Computational Intelligence Evolutionary Computation Proceedings*, IEEE Publ., Piscataway, NJ, 1998, pp. 218–223. doi:10.1109/ICEC.1998.699504

[9] Xue, M., "Three-Dimensional Sector Design with Optimal Number of Sectors," *Journal of Guidance, Control, and Dynamics*, Vol. 35, No. 2, 2012, pp. 609–618. doi:10.2514/1.51979

[10] Kicinger, R., and Yousefi, A., "Heuristic Method for 3-D Airspace Partitioning: Genetic Algorithm and Agent-Based Approach," *9th AIAA ATIO Conference*, AIAA Paper 2009-7058, 2009, pp. 1–0. doi:10.2514/6.2009-7058

[11] Li, J., Wang, T., Savai, M., and Hwang, I., "A Spectral Clustering Based Algorithm for Dynamic Airspace Configuration," *9th AIAA ATIO Conference*, AIAA Paper 2009-7056, 2009. doi:10.2514/6.2009-7056

[12] Xue, M., "Airspace Sector Redesign Based on Voronoi Diagrams," *Journal of Aerospace Computing, Information, and Communication*, Vol. 6, No. 12, 2009, pp. 624–634. doi:10.2514/1.41159

[13] Prete, J., and Mitchell, J., "Safe Routing of Multiple Aircraft Flows in the Presence of Time-Varying Weather Data," *AIAA Guidance, Navigation, and Control Conference and Exhibit Guidance, Navigation, and Control and Co-Located Conferences*, AIAA Paper 2004-4791, doi:10.2514/6.2004-4791

[14] Matthews, M. P., Veillette, M. S., Venuti, J. C., DeLaura, R. A., and Kuchar, J. K., "Heterogeneous Convective Weather Forecast Translation into Airspace Permeability with Prediction Intervals," *Journal of Air Transportation*, Vol. 24, No. 2, 2016, pp. 41–54. doi:10.2514/1.D0025

[15] Kicinger, R., Chen, J., Steiner, M., and Pinto, J., "Airport Capacity Prediction with Explicit Consideration of Weather Forecast Uncertainty," *Journal of Air Transportation*, Vol. 24, No. 1, 2016, pp. 18–28. doi:10.2514/1.D0017

[16] Krozel, J., Penny, S., Prete, J., and Mitchell, J. S., "Comparison of Algorithms for Synthesizing Weather Avoidance Routes in Transition Airspace," *AIAA Guidance, Navigation and Control Conference and Exhibit*, AIAA Paper 2004-4790, 2004. doi:10.2514/6.2004-4790

[17] Yang, S., Mitchell, J. S. B., Krozel, J., Polishchuk, V., Kim, J., and Zou, J., "Flexible Airlane Generation to Maximize Flow Under Hard and Soft Constraints," *Air Traffic Control Quarterly*, Vol. 19, No. 3, 2012, pp. 211–235. doi:10.2514/atcq.19.3.211

[18] Forster, C., Ritter, A., Gemsa, S., Tafferner, A., and Stich, D., "Satellite-Based Real-Time Thunderstorm Nowcasting for Strategic Flight Planning En Route," *Journal of Air Transportation*, Vol. 24, No. 4, 2016, pp. 113–124. doi:10.2514/1.D0055

[19] Hart, P. E., Nilsson, N. J., and Raphael, B., "A Formal Basis for the Heuristic Determination of Minimum Cost Paths," *IEEE Transactions on Systems Science and Cybernetics*, Vol. 4, No. 2, July 1968, pp. 100–107. doi:10.1109/TSSC.1968.300136

[20] Flener, P., and Pearson, J., "Automatic Airspace Sectorisation: A Survey," EUROCONTROL, Nov. 2012, http://www.it.uu.se/research/group/astra/publications/D2Y4.pdf.

[21] Bichot, C.-E., and Durand, N., "A Tool to Design Functional Airspace Blocks," *ATM 2007, 7th USA/Europe Air Traffic Management Research and Development Seminar*, Barcelona, 2007, pp. 169–177, www.atmseminar.org. doi:10.1.1.383.9367

[22] Sridhar, B., Sheth, K. S., and Grabbe, S., "Airspace Complexity and its Application in Air Traffic Management," *2nd USA/Europe Air Traffic Management R&D Seminar*, Orlando, FL, 1998, pp. 1–9, www.atmseminar.org.

[23] Tang, J., Alam, S., Lokan, C., and Abbass, H. A., "A Multi-Objective Evolutionary Method for Dynamic Airspace Re-Sectorization Using Sectors Clipping and Similarities," *IEEE Congress on Evolutionary Computation*, IEEE Publ., Piscataway, NJ, 2012, pp. 1–8. doi:10.1109/CEC.2012.6253008

[24] Deb, K., Pratap, A., Agarwal, S., and Meyarivan, T., "A Fast and Elitist Multiobjective Genetic Algorithm: NSGA-II," *IEEE Transactions on Evolutionary Computation*, Vol. 6, No. 2, April 2002, pp. 182–197. doi:10.1109/4235.996017

[25] Lin, S., "NGPM—A NSGA-II Program in Matlab v1.4 [online database]," MathWorks, Matick, MA, http://www.mathworks.com/matlabcentral/fileexchange/31166-ngpm-a-nsga-ii-program-in-matlab-v1-4 [retrieved 15 Aug. 2015].

C. Wanke
Associate Editor